Journal Pre-proof

A new bivalent fluorescent fusion protein for differential Cu(II) and Zn(II) ion detection in aqueous solution

A.E. Sorenson, P.M. Schaeffer

PII: S0003-2670(19)31453-9

DOI: https://doi.org/10.1016/j.aca.2019.12.017

Reference: ACA 237300

To appear in: *Analytica Chimica Acta*

Received Date: 25 July 2019

Revised Date: 6 December 2019

Accepted Date: 8 December 2019

Please cite this article as: A. Sorenson, P. Schaeffer, A new bivalent fluorescent fusion protein for differential Cu(II) and Zn(II) ion detection in aqueous solution, *Analytica Chimica Acta*, https://doi.org/10.1016/j.aca.2019.12.017.

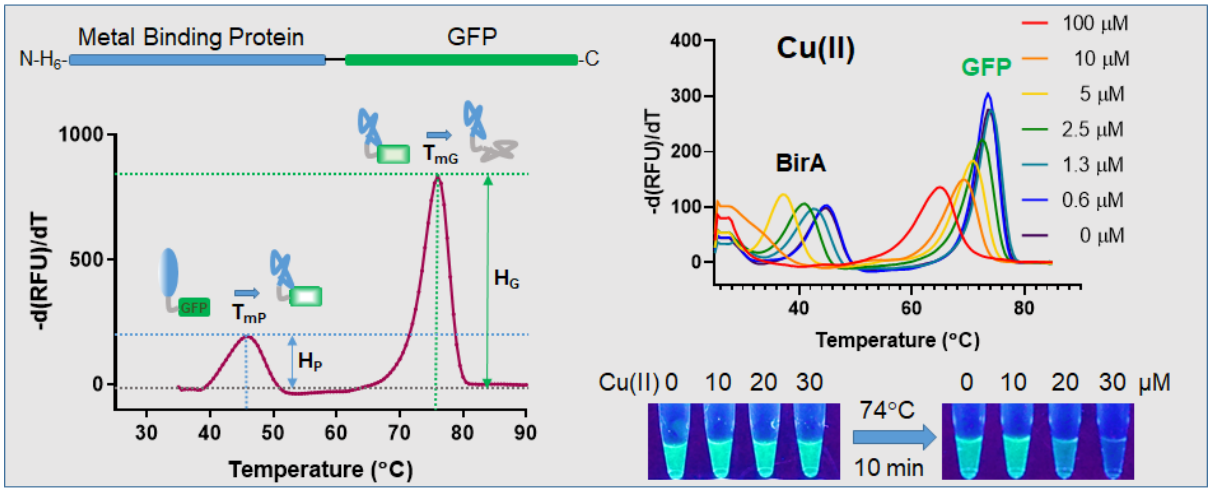

A new bivalent fluorescent fusion protein for differential Cu(II) and Zn(II) ion detection in aqueous solution

Sorenson AE[1]

Schaeffer PM[1]

[1] Molecular and Cell Biology, College of Public Health, Medical and Veterinary Sciences, James Cook University, Douglas QLD 4811, Australia

*Corresponding author

Associate Professor Patrick Schaeffer

Phone: +61 (0)7 4781 4448

Email: patrick.schaeffer@jcu.edu.au

Address: The Science Place, Building 142, University Drive, James Cook University, Douglas, Queensland 4811, Australia

Abstract

Simple and easy to engineer metal-sensing molecules that are capable of differentiating metal ions and producing metal-specific signals are highly desirable. Metal ions affect the thermal stability of proteins by increasing or decreasing their resistance to unfolding. This work illustrates a new strategy for designing bivalent fluorescent fusion proteins capable of differentiating metal ions in solution through their distinct effects on a protein's thermal stability. A new dual purpose metal sensor was developed consisting of biotin protein ligase (BirA) from *B. pseudomallei* (Bp) fused to green fluorescent protein (GFP). When coupled with differential scanning fluorimetry of GFP-tagged proteins (DSF-GTP) for signal-transduction detection, Bp BirA-GFP yields distinct protein unfolding signatures with Zn(II) and Cu(II) ions in aqueous solutions. The limit of detection of the system is ~1 μM for both metal species. The system can be used in a variety of high-throughput assay formats including for the screening of metal-binding proteins and chelators. Bp BirA-GFP has also the additional benefit of being useful in Cu(II) ion field-testing applications through simple visual observation of a temperature-dependent loss of fluorescence. Bp BirA-GFP is the first example of a protein-based dual purpose Cu(II) and Zn(II) ion sensor compatible with two different yet complementary signal-transduction detection systems.

Key Words

Differential scanning fluorimetry; DSF-GTP; zinc; copper; chemodosimeter; biosensor; biotin protein ligase; green fluorescent protein; HIV integrase; DnaG primase; DNA ligase; Dengue RNA-dependent-RNA-polymerase; Burkholderia; Mycobacterium

1. Introduction

Transition metals such as zinc, copper and iron are essential biological microelements and their concentration must be tightly regulated to avoid deficiencies or toxic effects in living organisms. The presence of Zn(II) ions in tap water indicates corrosion of copper pipes but it is not linked to health or safety concerns [1]. However elevated copper intake can lead to gastrointestinal symptoms and liver toxicity and can adversely affect individuals carrying the Wilson disease gene and children predisposed to childhood copper cirrhosis syndromes [2]. Sensitive detection of transition metals in environmental and biological samples requires complex analytical instruments such as atomic absorption, and inductively coupled plasma mass spectrometers. Electrochemical methods are also commonly used. They require simpler instruments that are easier to use but they suffer from a lower detection sensitivity [3]. Alternatively, colorimetric or fluorescent metal chemosensors and chemodosimeters [4, 5] can be used with variable sensitivity and selectivity. These often lack specificity and require masking agents for other biologically relevant metal ions such as iron and copper. Colorimetric kits are routinely used to detect Zn(II) ions in serum and urine.

Biosensors consist of a metal-binding biomolecule and a signal transduction system. DNA-, RNA- and protein-based sensors have been described for a large panel of metal ions [6-11]. Carbonic anhydrase-based systems are most sensitive for detection of Cu and Zn [12]. Protein-based metal biosensors often include a fluorescent reporter system for detection [13-16]. DsRed has been shown to detect as little as 10 nM of Cu(I) or (II) ions [13]. A histidine modified eGFP was engineered that can sense a concentration of 10 nM of Cu(II) ions [17]. Another reengineered GFP includes a metal coordination site and was shown to be highly sensitive to Pb ions at micromolar concentrations [18]. Metal ion quenchable fluorescent proteins that are uniquely modulated by Cu(II), Ni(II), Co(II) and Zn(II) ions have been developed as biosensors and imaging probes [19]. Fully synthetic blue fluorescent protein

analogs were recently developed as Zn(II) chemosensors [16]. Unfortunately, although very sensitive, most chemo- or biosensor transduced signals cannot distinguish between metal ions when detectable levels of interfering metal ions are present.

Simple and easy to engineer metal-sensing probes that are capable of identifying more than one metal ion and producing metal-specific signals are highly desirable. Along these lines, a GFP chromophore inspired chemosensor was successfully developed that is capable of simultaneous determination of Hg(II) and Zn(II) ions [20]. A quinolinyl-substituted anthracenone can be used either as a chemosensor for Zn(II) or a chemodosimeter for Cu(II) via two independent chemical mechanisms [21]. More recently, a pyridoxal-based dual chemosensor was engineered for both visual detection of Cu(II) and ratiometric fluorescent detection of Zn(II) [22]. Developing such designer molecules with desired properties and solubility remains challenging.

Metal-binding proteins containing zinc fingers [23, 24] are well suited to be genetically engineered into biosensors and chemodosimeters [25]. Here again, reengineering these proteins with desired properties is not easy. Transition metals affect the stability of proteins by increasing or decreasing their unfolding temperature. Although metal ion binding to a protein can easily be measured by differential scanning calorimetry or differential scanning fluorimetry (DSF), such techniques have not yet been exploited as an integrated signal transduction and detection system. Recent developments such as DSF-GTP [26-28] and the principle of selective protein unfolding [29] inspired us to evaluate a selection of metal-binding proteins tethered to GFP as metal ion sensing probes. Unexpectedly, this proof of concept study identified the recently characterized *Burkholderia pseudomallei* (Bp) biotin protein ligase (BirA) [30] as a sensitive metal-sensing protein capable of detecting and differentiating Zn(II) and Cu(II) ions in aqueous solution when tethered to GFP.

2. Material and methods

2.1 Cloning, expression and purification

Bp DnaG-GFP and DENV RdRp-GFP were produced as described previously (Moreau et al., 2012). Ec BirA-GFP [31], Bp BirA-GFP [30] and Mt BirA-GFP [32] were produced as described previously. For Bp LigA-GFP and HIVint-GFP, *E. coli* expression codon optimized Bp LigA and HIVint coding sequences (Bioneer) were cloned into pIM013 (pET-uvGFP) [33] to create pAC284 (pET-N-6His-HIVint-GFP-C) and pAC292 (pET-N-6His-BpLigA-GFP-C). Bp LigA-GFP was expressed in *E. coli* BL21(DE3)RIPL using Overnight Express TB Medium (Novagen) containing 100 µg mL^{-1} ampicillin and 50 µg mL^{-1} chloramphenicol. Cultures (100 mL) were incubated at 37 °C with shaking until OD_{600} reached 0.5, then reduced to 16 °C for a further 2.5 days. HIVint-GFP was expressed in *E. coli* KRX using standard TB medium containing 100 µg mL^{-1} ampicillin. Cultures (100 mL) were incubated at 37 °C with shaking until OD_{600} reached 1.5, then induced with 0.1% rhamnose and reduced to 16 °C for a further 24 hr. Lysis and purification procedures were performed as previously described [26, 34]. All proteins were stored in 50 mM phosphate buffer, pH 7.8 with 300 mM NaCl, 20 mM imidazole, 2 mM β-mercaptoethanol and 10% glycerol at concentrations ranging between 50-100 µM. Protein concentrations were determined by Bradford assay and GFP fluorescence. Protein integrity and purity were assessed by SDS-PAGE.

2.2 DSF-GTP melt curve experiments

All DSF-GTP [26, 28] melt curve experiments were run in sealed 96-well, hard-shell, skirted PCR plates (Bio-Rad) with a CFX-96 (Bio-Rad) thermal cycler to determine transition midpoints values for both test protein (T_{mP}) and reference GFP (T_{mG}). Melt curves were

generally run unless otherwise stated from 25-90°C, in 0.5 °C increments for 30 s using the FAM channel. Changes in T_m (ΔT_{mP} and ΔT_{mG}) values were determined for each reaction condition compared to a control reaction. For protein refolding analyses two successive DSF-GTP melt curves were run, with the first one from 25-60°C, followed by a second one from 25-90°C. Specific DSF-GTP protocols and reagents list are detailed in the ESI.

2.3 GFP-Basta for determination of protein aggregation

GFP-Basta experiments were analysed in sealed 96-well, hard-shell, skirted PCR plates (Bio-Rad) with a CFX-96 (Bio-Rad) thermal cycler to measure a sample's GFP fluorescence (initial and residual after centrifugation) using a 2-min run at 25°C using the FAM channel. Centrifugation of samples was routinely performed in 8-well PCR strips at 18,000x*g* for 15 min at 4°C. Metal ion-induced protein aggregation (i.e. with Zn(II) acetate or Cu(II) sulphate) was determined using a protocol similar to a previously described method [33]. The initial fluorescence of a fusion protein (at 1 µM in 25 mM ammonium sulphate (pH 5.7) and 5% glycerol) was first measured in each sample in the presence and absence of 12.5 µM Zn(II) or Cu(II) ions. Samples were then gradually heated from 25°C to a temperature corresponding to the start or end of their respective protein T_{mP} peaks in the CFX-96 thermal cycler in 0.5°C increments for 30 s using the FAM channel. Heated samples were centrifuged and the supernatants transferred to a fresh 96-well plate for measurement of the residual fluorescence in each sample. All reactions were performed in triplicate.

2.6 Blind water testing

Equal volumes of Bp BirA-GFP at 1 µM in 50 mM ammonium sulphate (pH 5.7) and 10% glycerol were mixed with equal volumes of serial dilutions of tap water (laboratory recycled system diluted in milli Q water) with and without 125 µM EDTA. Melt curves were performed, followed by T_m and ΔT_m determination. Reactions were performed in triplicate.

The same water sample was independently tested for elemental analysis and quantitation by ICP-MS at the Advanced Analytical Centre, James Cook University.

2.7 Spike and recovery accuracy assessment

Equal volumes of Bp BirA-GFP at 1 µM in 50 mM ammonium sulphate (pH 5.7) and 10% glycerol were mixed with equal volumes of water samples (two commercial drinking water samples from different suppliers and one freshwater creek sample) with no added metal ion, or spiked with Zn(II) and Cu(II) ion solutions to final concentrations of 10, 20 and 30 µM. Standards were prepared by mixing 90 µL of 5 mM sodium bicarbonate with 10 µL metal ion solutions (pH 8.6). Spiked water samples were prepared in the same way. Melt curves were performed, followed by T_m and ΔT_m determination. Reactions were performed in triplicate along with standard curves for each metal from 0-70 µM.

2.8 Isothermal Cu(II)-dependent fluorescence quenching format for field water testing

Equal volumes of Bp BirA-GFP at 4 µM (in 50 mM ammonium sulphate (pH 5.7) and 10% glycerol) and Cu(II) sulphate solutions at 30, 20 and 10 µM were mixed and heated for 10 min in a temperature gradient ranging from 65-85°C with a thermocycler (Kyratec Supercycler). Samples were simply visualized over a UV transilluminator at 365 nm. Alternatively a CFX96 thermal cycler with monitoring set to the FAM channel was used as indicated with readings taken prior to heating, and at 30 s intervals throughout the 10 min incubation (*cf* ESI for detailed methods).

3. Results and discussion

Metal-binding protein evaluation and selection

Differential scanning fluorimetry of GFP tagged proteins (DSF-GTP) has been successfully applied to the characterization of protein-ligand interactions and as a high-throughput assay

for small molecule library screening [26, 27, 29-32]. The method allows real-time monitoring of the unfolding of a test protein tethered to GFP (Fig 1). The temperature-dependent unfolding and aggregation of the test protein leads to a measurable reduction in GFP fluorescence that can be transformed into a transition midpoint (T_{mP}) peak followed by a second one when the GFP unfolds (T_{mG}). Over the years, we have screened several fluorescent fusion proteins, including putative and well-characterized metal-binding proteins with a range of salts and buffer systems for their optimal storage. We noted significant and distinct changes in T_m for both test proteins and GFP, and their respective fluorescence intensity (H_P and H_G), especially with Zn(II) and Cu(II) ion solutions. These observations prompted us to evaluate the potential of DSF-GTP with a selection of metal-binding proteins fused to GFP as a new approach for the quantitation of Zn(II) and Cu(II) ions in aqueous solutions (Fig 1).

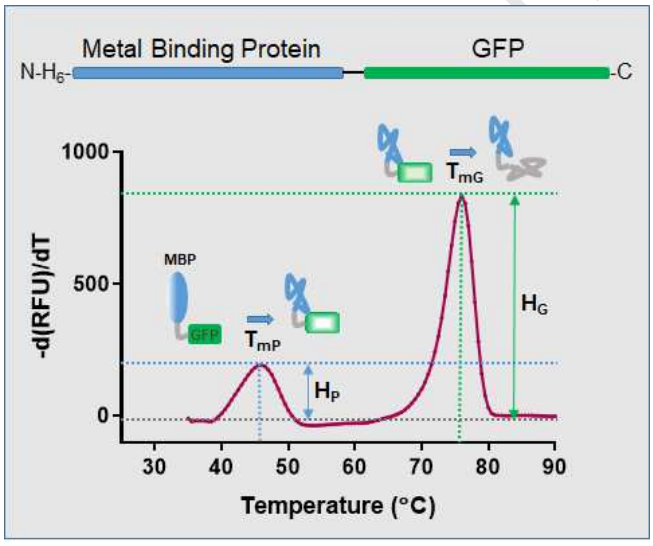

Figure 1: General principle of a bivalent fluorescent fusion protein metal sensor. The fluorescent fusion protein consists of an N-terminal hexahistidine (H_6) tag followed in order by the metal-binding protein, short linker and C-terminal GFP sequences. The fluorescent fusion protein is gradually heated leading to unfolding of the metal-binding protein (MBP) followed by unfolding of GFP. A typical DSF-GTP melt curve is shown for a candidate

fluorescent fusion protein. The curve shows a typical transition midpoint of unfolding for MBP (T_{mP}) and another for GFP (T_{mG}). Metal ions interacting with the MBP and GFP will lead to measurable concentration-dependent changes in T_{mP}, T_{mG}, H_P and H_G values. In principle, specific and measurable changes in at least two of these parameters would be required for sensitive and selective metal ion detection and identification.

HIVint-GFP and RdRp-GFP [26, 29] were selected due to the presence of one Zn binding motif in the HIVint domain [35] and two well characterized Zn binding motifs in the RdRp domain [36]. Bp DnaG-GFP [29] and LigA-GFP were selected due to a predicted Zn finger in their respective sequences. Ec, Bp and Mt BirA-GFP [30-32] were chosen as control proteins due to the absence of zinc binding motifs in their sequences. All fluorescent fusion proteins were expressed and purified using a standard method and buffer for comparative evaluation [29]. Metal-binding proteins were not assessed with regards to their metal content in the initial evaluation. DSF-GTP melt curves were run from 25-90°C yielding distinct T_{mP} and T_{mG} for each test protein and GFP. HIVint-GFP, although soluble and fluorescent, yielded a very weak T_{mP} peak and was thus abandoned. All remaining fusion proteins produced distinct T_m peaks for the test protein and GFP as well as significant H_P/H_G ratios > 0.25 (Table S1 and Fig S1). We confirmed that the test proteins did not refold after running a partial DSF-GTP melt curve spanning from 25-60°C prior another full run from 25-90°C.

All fusion proteins were interrogated in parallel with Zn(II) acetate and Cu(II) sulfate solutions ranging from 3.1 to 12.5 µM (Fig S1). The T_{mG} peaks for GFP shifted consistently towards lower temperatures in a concentration-dependent manner with Cu(II) but no significant shift was observed with Zn(II) ions. For Bp DnaG-GFP, RdRp-GFP and Ec BirA-GFP, the presence of 3.1 µM of Zn(II) or Cu(II) led to near complete or total loss of their T_{mP} peaks. Bp LigA-GFP was the only putative zinc-binding protein that showed a gradual concentration-dependent T_{mP} shift towards lower temperature for both Zn(II) and Cu(II) ions.

The T_{mP} peaks of Bp, Ec and Mt BirA-GFP orthologs were differently affected by increasing Zn(II) and Cu(II) ion concentrations. Mt BirA-GFP T_{mP} was almost unaffected by both metal ions. Surprisingly, Bp BirA-GFP showed significant gradual T_{mP} shifts towards lower temperature with increasing Zn(II) and Cu(II) ions. Bp BirA-GFP has recently been characterized but no structural data is available for Bp BirA [30]. Examination of the amino acid sequence of Bp BirA revealed the presence of two proximal cysteines (**C**SVA**C**) in its N-terminal region and two proximal histidines (**H**AL**H**) in its C-terminal region that resemble zinc binding half-sites [37]. However, modelling of the Bp BirA structure did not indicate that any of these motifs are in close proximity to each other (Fig S2). CXXXC motifs have also been found to bind copper in conjunction with a distant histidine residue [38]. Within Bp BirA, it is possible that further metal coordinations could occur through interaction with suitable ligands.

We confirmed that for all test proteins and GFP, the T_m shifts as well as the reduction or loss of T_{mP} peak amplitude H_P were due to metal ion binding by reversing their effect in the presence of excess EDTA (Fig S3). We did not observe any significant change in T_{mP} peak for any of the zinc-binding proteins in the presence of excess EDTA, which was rather surprising as it is capable of stripping Zn(II) ions from many proteins [39]. Our data suggest that these proteins are not bound to zinc. Furthermore, we show that for RdRp and DnaG, the reduction or loss of T_{mP} peak amplitude is due to Zn(II) and Cu(II) induced protein aggregation (Fig S4). It seems that for HIVint-GFP, Zn(II) binding also leads to protein aggregation but this could not be confirmed due to its very small T_{mP} peak H_P amplitude. The significant thermal destabilization and protein aggregation observed at relatively low Zn(II) ion concentrations for all tested proteins containing Zn binding motifs is rather intriguing. The data suggest that Zn(II) ions bind and destabilize the unfolded state of these proteins. Most of the literature is replete with structural and stability data of Zn binding protein [24]

but there is little data describing protein destabilization effects upon Zn(II) ion binding. As an example, Zn(II) ion binding to the HCCH motif of HIV-1 virion infectivity factor leads to protein aggregation [40]. Zn(II) ions have also been shown to preferentially bind the unfolded state of the porcine growth hormone protein leading to its thermal destabilization [41]. Our data adds to the growing list of Zn(II) ion induced protein unfolding and aggregation.

This preliminary evaluation elevated Bp BirA-GFP as the most promising metal-sensing protein candidate due to its large T_{mP} peak and H_P values, and its progressive but strikingly different T_{mP} and T_{mG} peak downshifts that were obtained with increasing Zn(II) and Cu(II) ion concentrations. In fact, it became evident that Bp BirA-GFP could not only be used to detect and quantitate Zn(II) or Cu(II) ions in aqueous solution but it may also offer the possibility of differentiating these two M(II) ions.

Validation of Bp BirA-GFP as a dual Zn(II) and Cu(II) ion sensor

We evaluated serial dilutions of Zn acetate and $CuSO_4$ to determine the sensitivity of Bp BirA-GFP (Fig 2). It was possible to measure significant T_m peaks with 0.5 µM of Bp BirA-GFP and T_m downshifts with as little as 1 µM of Zn(II) and Cu(II) ions in aqueous solutions. The effects of Zn(II) and Cu(II) ions on Bp BirA and GFP were further analysed by plotting their respective ΔT_m as a function of [M(II)] and log[M(II)] (Fig 2). These plots revealed distinct metal-specific inflection starts, shapes and slopes, thus allowing not only the determination of M(II) ion concentration in solution but also their identification. In the case of Zn(II) ions a 1:1 binding mode is most likely to occur based on the progressive T_m curves and hyperbolic ΔT_m as a function of [Zn(II)] plot (Fig 2A-C). On the other hand, it is obvious that Cu(II) ions bind more than one site with different affinity on Bp BirA based on the melt curves and the apparent pseudolinear ΔT_m as a function of [Cu(II)] plot (Fig 2D-E). The striking nonlinear bimodal ΔT_m as a function of log[Cu(II)] plot suggests two distinct slopes,

supporting that Bp BirA has at least two different binding sites with different affinities for Cu(II) ions (Fig 2F). It is possible that upon partial unfolding a new binding site is exposed. The **C**SVA**C** motif could potentially interact with a histidine present in the N-terminal region. Additional ligand atoms observed in copper binding proteins can be provided by other residues such as methionine, glutamine and leucine [42]. Another intriguing phenomenon is the sudden increase in T_m amplitude ratio at higher Cu(II) ion concentration (Fig 2D). We are not sure as to why this happens (*cf* with the gradual decline in T_m amplitude ratio with Zn(II) in Fig 2A) but it offers a practical visual means to distinguish the metal species in solution. Most importantly, the different standard curves and lines obtained for ΔT_{mP} and ΔT_{mG} (Fig 2 and Table S2) offer flexibility for data fitting, an extended linear range and a high-level of confidence at concentrations where both ΔT_{mP} and ΔT_{mG} reference lines can be used for M(II) ion determination. This is particularly evident in the case of Cu(II) sensing were both reference lines for ΔT_{mP} (*cf* Fig 2E) and ΔT_{mG} (*cf* Fig 2F) can be used to determine the concentrations of Cu(II) ions ranging from ~1-10 µM. Bp BirA-GFP is the first example of a protein-based dual purpose Cu(II) and Zn(II) ion sensor offering two different yet complementary signal detection strategies.

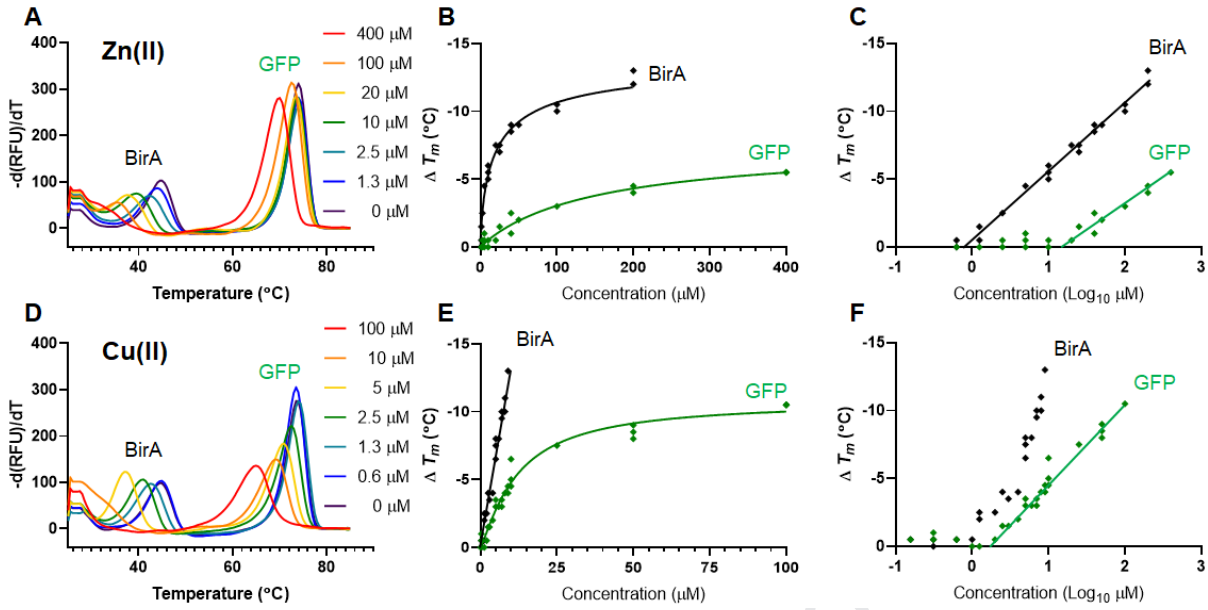

Figure 2: Thermal destabilization of Bp BirA-GFP in response to Zn(II) and Cu(II) ions. A) DSF-GTP melt curve signature obtained with increasing Zn(II) ion concentrations. ΔT_{mP} and ΔT_{mG} values obtained with increasing concentrations of Zn(II) ions **(B)** and semi-log plot representation **(C).** DSF-GTP melt curve signature, ΔT_{mP} and ΔT_{mG} values in linear and semi-log plot representation obtained with increasing Cu(II) ion concentrations **(D-F)**. Bp BirA-GFP at 0.5 µM in 25 mM ammonium sulphate (pH 5.7) and 5% glycerol in triplicate for each M(II) ion concentration. Data are presented using GraphPad Prism 8 with all data points included. Semi-log plots for Zn(II) ions **(C)** and Cu(II) ions **(F)** indicate different Bp BirA-GFP binding modes for these species. Data were fitted to a one site – specific binding model.

Metal selectivity and buffer effects

The utility of a metal sensor is limited by its metal selectivity. We assessed if other metal ions could significantly affect the T_m of Bp BirA-GFP. The effect of ^{37}Rb(I),^{12}Mg(II) and ^{20}Ca(II) ions as well as a selection of transition metal ions (i.e. ^{25}Mn(II), ^{26}Fe(II), ^{26}Fe(III), ^{27}Co(II), ^{28}Ni(II), ^{29}Cu(II), ^{30}Zn(II) and ^{42}Mo(VI)) were examined. At the metal ion concentration

shown (12.5 µM final) only Fe(II) ions slightly affected the T_{mP} of Bp BirA (Fig 3A). The limits of detection were similar for both Cu(II) and Zn(II) ions (Fig 3B).

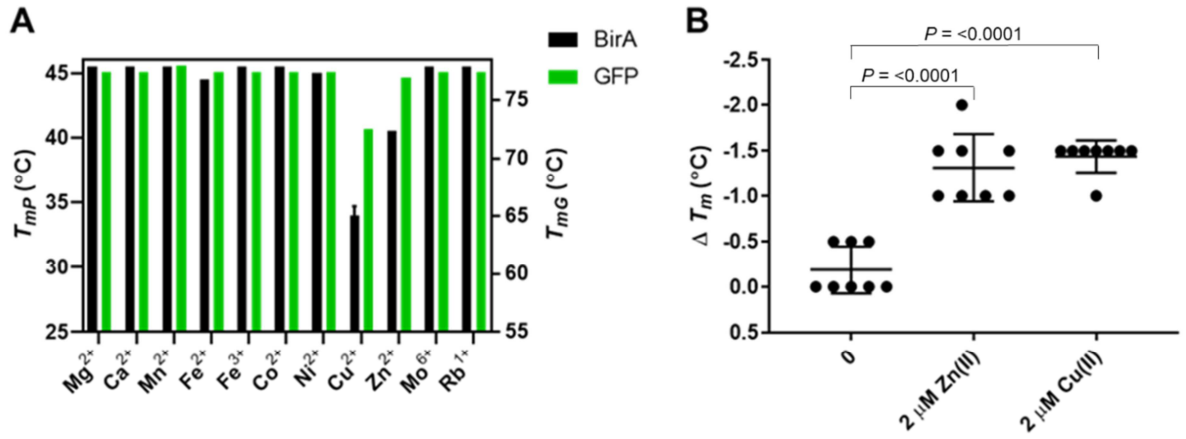

Figure 3: Metal ion selectivity of Bp BirA-GFP. A) Average T_m values were determined from melt curves with Bp BirA-GFP at 1 µM in the presence of 12.5 µM metal ions (N=2). T_{mP} axis is on the left and T_{mG} axis is on the right. **B)** The limit of metal ion detection was determined with 0.5 µM BirA-GFP. Eight reactions were run to determine the SD of no metal ions (±0.259) and compared with the same number of reactions containing metal ions. Statistical analyses were performed using Welch's t-test with GraphPad Prism 7.04. Here the concentrations are shown as initial metal ion concentrations in water samples before dilution with Bp BirA-GFP (1 µM). Final reaction concentrations for the metal ions and protein are half the values shown i.e. 1 µM which is also the absolute limit of detection for both metal ions.

We tested a series of ammonium sulphate, sodium phosphate, gluconate and citrate buffers and additives with pH ranging from 5.7-8.7 to examine their effect on the T_{mP} and T_{mG} as well as the metal sensitivity and selectivity of Bp BirA-GFP. In general, buffers did not significantly affect T_{mP} and T_{mG} with the exception of a phosphate buffer at pH 5.7 that downshifted the T_{mP} of Bp BirA-GFP (Fig S5). All phosphate buffers dramatically reduced

the sensitivity of Bp BirA-GFP to Cu(II) and Zn(II) ions due to formation of insoluble phosphate salts. Indeed, copper and zinc phosphate salts are mostly insoluble at all pH. We examined if the use of organic carboxylates as buffering agents could specifically affect the metal ion effect of either species on Bp BirA-GFP. The citrate buffer at pH 6 completely eliminated the effect of Zn(II) ions on Bp BirA. However, a small effect was still visible on Bp BirA with Cu(II) but not on GFP. A competing citrate metal ion chelating effect is most likely the reason for our data [43, 44]. The gluconate buffer at pH 5.7 did not seem to affect the effect of Zn(II) ions on Bp BirA nor GFP. However, it somewhat affected the effect of Cu(II) ions on Bp BirA and GFP. None of these buffers were found to improve the metal sensitivity or selectivity of Bp BirA-GFP and were not further investigated.

The addition of biotin increases significantly the T_{mP} of Bp BirA-GFP without affecting its T_{mG}. This is due to changes in protein conformation similar to the one seen in Ec BirA upon binding of biotin [30]. Biotin does not interact with Zn(II) nor Cu(II) ions (Fig 4A-B; *cf* green dashed vs full curves for GFP). The binding of biotin significantly reduced the magnitude of Zn(II)-induced thermal destabilization of Bp BirA (i.e. ΔT_{mP}) in Bp BirA-GFP. The conformational changes induced by the binding of Bp BirA to biotin increased the protein's stability and resistance to unfolding without significantly affecting its affinity for Zn(II) ions. It can be concluded that the binding sites for biotin and Zn(II) ions are not overlapping in Bp BirA. No further conclusion could be inferred about the topology of the Zn(II) metal ion binding site in Bp BirA.

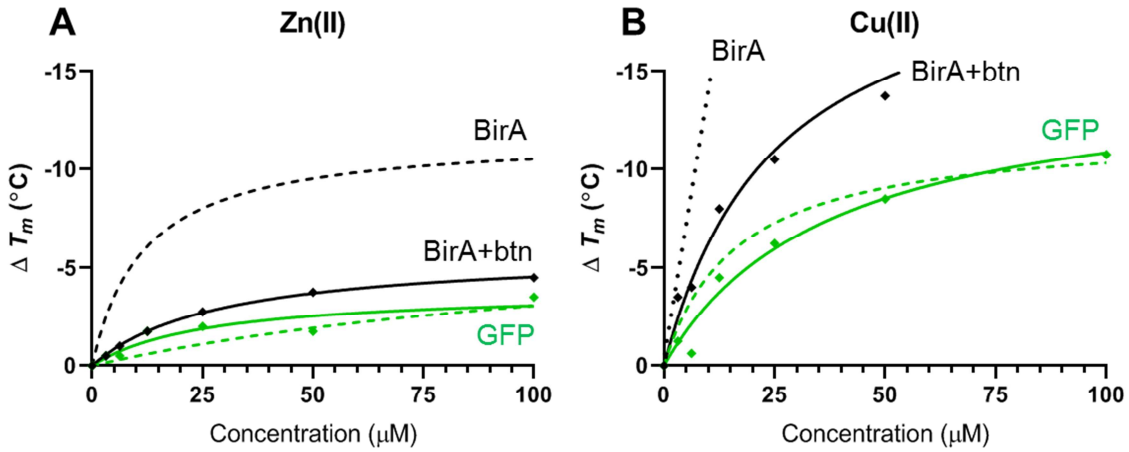

Figure 4: Zn(II) and Cu(II) ion binding of free and biotin-bound Bp BirA-GFP. The ΔT_{mP} and ΔT_{mG} values of free and biotin-bound Bp BirA-GFP with increasing concentration of Zn(II) ions **(A)** and Cu(II) ions **(B)**. T_m values were obtained with 0.5 µM Bp BirA-GFP in the presence or absence of 0.5 mM biotin (btn) as indicated. Metal ion concentrations are indicated on the abscissa. Dashed curves represent ΔT_m values obtained in the absence of btn (*cf* Fig. 2). All average values of ΔT_m are presented using GraphPad Prism 8 (N=3). Data were fitted to a one site – specific binding model or a straight line.

The binding of Bp BirA to biotin also affected its binding with Cu(II) ions (Fig 4B). Indeed, the striking pseudolinear ΔT_m as a function of [Cu(II)] plot obtained for free Bp BirA-GFP suggesting two different Cu(II) ion binding sites in Bp BirA is no longer observed (*cf* Fig 2E). Instead, a classic curve was obtained for biotin-bound Bp BirA-GFP, suggesting that only one Cu(II) ion can bind to biotin-bound Bp BirA (Fig 4B). However, it is not possible to assert if this interference with one of the Cu(II) ion binding sites is of a direct or indirect nature based on the data. It is safe to conclude that Bp BirA-GFP reacts very differently with Zn(II) and Cu(II) ions supporting different metal-binding topologies and modalities for these two species (Fig 2). In addition it would seem likely that biotin could be used to help differentiate Zn(II) and Cu(II) ions in a mixed sample, especially at low Zn(II) concentrations (*cf* Fig 4A and B).

Water testing

Next, we evaluated the utility of Bp BirA-GFP for water testing. For this, tap water was collected in our laboratory, serially diluted in milliQ water and tested with Bp BirA-GFP and DSF-GTP. Based on the T_{mP} and T_{mG} signature that we obtained, we concluded that Zn(II) ions were present. A control experiment in the presence of excess EDTA supported that the ΔT_m were due to M(II) ions in the water. We estimated a concentration of 27 ± 4 µM of Zn(II) ions in the tap water sample based on the slopes obtained by plotting ΔT_m as a function of log[M(II)] (Fig S6). Elemental analysis of the same water sample from the same container was independently performed by ICP-MS. The semi-quantitative ICP-MS scan indicated the presence of 13 µM Zn and 1.3 µM Cu in the tap water as well as significant concentrations of other metal species, including known signal suppressants such as sodium (Table S3). Based on the ICP-MS data, the highest possible final concentration of Cu in our reaction setup was 0.65 µM which would be near the limit of detection of Bp BirA-GFP (Fig 3B) and would only have minimally affected the T_{mP} and T_{mG} values. We concluded that the presence of all other metal and counter ion species in the tap water did not significantly affect the T_{mP} or T_{mG} of Bp BirA-GFP. The recommended maximum impurity concentrations (RMIC) for Cu in Australia is 2 mg L^{-1} corresponding to 31.5 µM and 3 mg L^{-1} for Zn equating to 45.9 µM. Bp BirA-GFP is thus sensitive enough to be applied in water testing [1]. Real-time PCR is increasingly applied to detect microbial contaminants in routine water testing. We envisage that Bp BirA-GFP could easily be implemented as a cost effective alternative to ICP-MS for Zn and Cu testing in water testing facilities with real-time PCR capability. The current DSF-GTP format allows testing of 96 samples in each run with a duration of ~90 min from sample preparation to analysis.

For accuracy evaluation using spike and recovery assessment, three different water sources were used (*cf* Table S4 for main ion water composition). Water samples were spiked with

increasing metal ion concentrations ranging from 0-30 µM (Table 1). Reference metal ion standards contained 4.5 mM sodium bicarbonate (pH 8.6) and were fit using a linear regression model *(cf* Fig S7). The recovery (%) for all spiked concentrations and water sources that were tested ranged from 84-119% with an average of 102.1 ± 9.2%, highlighting a satisfactory metal ion detection accuracy of Bp BirA-GFP for both Zn(II) and Cu(II) species (Table 1 and Fig S8).

Table 1: Spike and recovery of Zn(II) and Cu(II) ions in three different water samples

M(II) ion	*µM*	Source 1		Source 2		Source 3		Source 1-3	
		detected µM	***recovery %***	***detected µM***	***recovery %***	***detected µM***	***recovery %***	***p-value***	***95% CI***
Zn	10	10.1 ±1.5	101	10.5 ±0.9	105	10.7 ±1.6	107	BirA 0.0548	9.9-10.9
	20	19.0 ±1.7	95	18.3 ±2.7	92	20.3 ±1.8	102	BirA 0.0453	18.5-20.0
	30	27.3 ±1.7	91	27.8 ±1.0	93	29.3 ±2.2	98	BirA 0.0001	27.7-29.0
	10	10.4 ±1.1	104	11.7 ±1.4	117	11.7 ±1.9	117	BirA 0.0001	10.7-11.8

Cu	20	8.4 ±1.0	84	11.9 ±1.5	119	11.0 ±1.6	110	GFP 0.0880	9.9-11.5
		18.9 ±1.9	94	21.6 ±1.9	108	21.8 ±2.7	109	BirA 0.1183	19.8-21.7
		18.1 ±2.1	91	21.2 ±2.7	106	19.2 ±1.7	96	GFP 0.1865	18.2-20.4
	30	27.6 ±2.3	92	30.1 ±0.8	100	33.4 ±1.5	111	BirA 0.1253	29.7-32.0
		33.2 ±2.1	111	32.5 ±4.9	108	28.8 ±1.8	96	GFP 0.0266	30.2-33.2

Water samples were assayed by adding spike stock solutions calculated to yield the intended spike concentrations. Recoveries for spiked test samples were calculated by comparison to the measured recovery of spiked control in reaction buffer. All values represent the average of four independent repeats with samples in triplicate for each spike concentration (N=12). The p-values were determined using all the dataset (i.e. water sources 1-3) for each spike concentration (N=36). In the case of Cu(II) ions spike, concentrations were determined with BirA as well as GFP standard curves separately (cf Fig S7C-D). One-sample t-tests were performed using GraphPad Prism 7.04 (cf Fig S8).

The obvious temperature-dependent increased Cu(II) ion sensitivity of GFP prompted us to evaluate the applicability of our fluorescent fusion protein in a simple isothermal Cu(II)-dependent fluorescence quenching format for field water testing (Fig 5A). Here, the experimental setup involves mixing of the Cu(II) solution and Bp BirA-GFP followed by a 10-min heat treatment and comparison of the residual fluorescence against a standard.

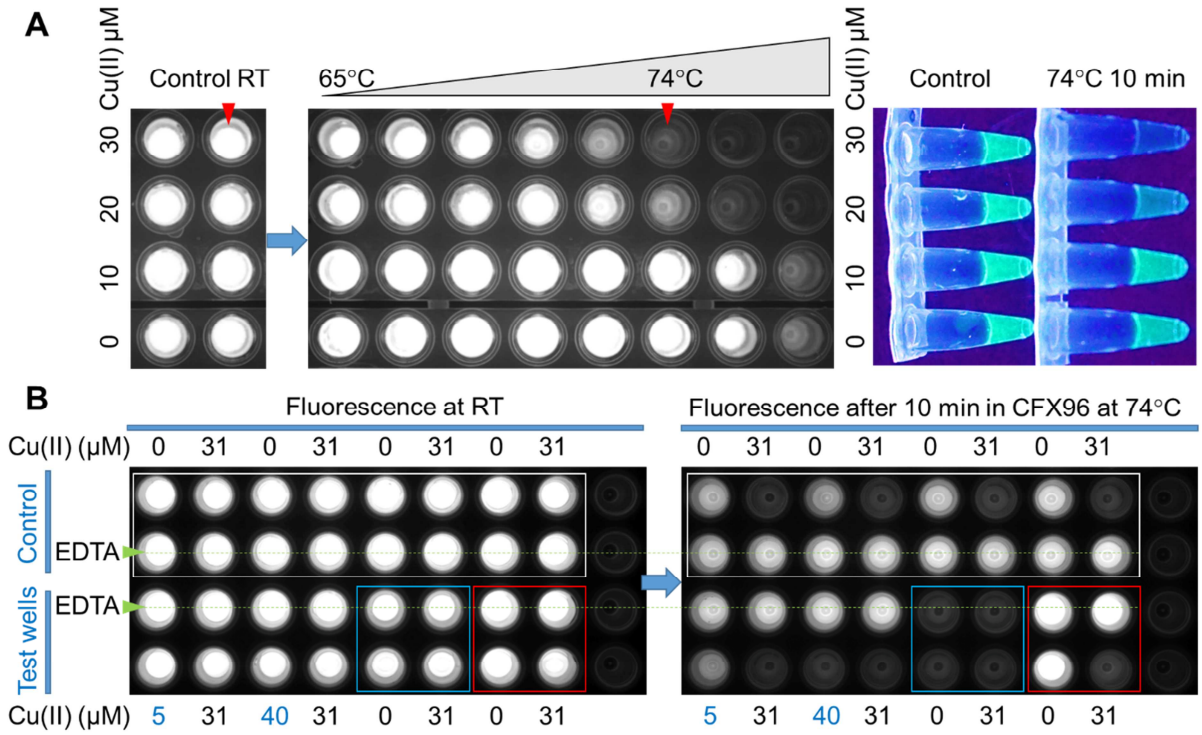

Figure 5: Temperature-dependent fluorescence responses of Bp BirA-GFP to Cu(II) ions in water. A) Top view of a 2-dimensional grid examining the effect of increasing concentrations of Cu(II) ions and temperature on GFP fluorescence (as indicated in grey scale). Red arrowheads indicate the residual fluorescence in the same wells before and after heating. The colour photographs on the right, represent a visual examination of the samples with UV transillumination at 365 nm showing the gradual loss of GFP fluorescence with increasing concentrations of Cu(II) ions after 10 min incubation at 74°C. Equal volumes of Cu(II) ion solutions (0-30 µM) and Bp BirA-GFP (4 µM) were mixed. RMIC for Cu(II) ions is 31 µM. **B)** Simplified field testing matrix with control (top rows, white quadrant) and test

wells (bottom rows) in the presence or absence of EDTA (100 µM final as indicated by green arrowheads and dashed lines) Black numbers represent the initial Cu(II) ion concentrations in the water sample and control wells before dilution with Bp BirA-GFP. Blue numbers are the initial concentrations of Cu(II) ions in spiked test water samples. Blue quadrants show limits of testing conditions in acidic conditions (pH 4.9). Red quadrants show increased stability of Bp BirA-GFP due to the presence of 5 mM bicarbonate and increased pH in the water sample (pH 8.6).

To further evaluate the limits of the isothermal Cu(II)-dependent fluorescence quenching format for field water testing, we determined the maximum concentrations of Ni(II), Fe(II) and Zn(II) ions that will interfere with the performance of the test. First, we performed a series of DSF-GTP melt curve experiments in the presence of increasing concentrations of Zn(II) with either Cu(II), Fe(II) or Ni(II) as well as Cu(II) with either Zn(II), Fe(II) and Ni(II) ions (Fig S9A). For most combinations of metal ions, the data suggest a simple cumulative effect model on T_{mP} and T_{mG}. The presence of Ni(II) ions (up to 100 µM final reaction concentration) showed very little effect on T_{mP} and T_{mG} (≤ 1°C) that would fall below the LOD for Cu(II) and Zn(II) ions. The presence of Fe(II) ions ≤ 25 µM also showed very little effect on T_{mP} and T_{mG} (≤ 1°C). The Zn(II) ion concentration cannot be determined in the presence of significant concentrations of Cu(II) ions as the latter are clearly dominant in their effect on T_{mP} and T_{mG}. Then we examined the effect of increasing concentrations of Cu(II) ions and temperature on GFP fluorescence in the presence or absence of 50 µM of either Fe(II) or Zn(II) ions in the water sample using a 2-dimensional fluorescence quenching grid format (Fig S9B). The data support the utility of the isothermal Cu(II)-dependent fluorescence quenching format for field water testing in the presence of ≤ 50 µM of either Fe(II) or Zn(II) ions in the water sample.

Finally, we designed a matrix that would allow identification of interfering conditions upon testing a water sample by introducing several controls including a metal ion reversal well (EDTA) and a 30 µM Cu(II) ion well (Fig 5 B). Acidic pH and increased pH due to the presence of bicarbonate were tested as potential interfering conditions. As expected acidic pH totally invalidated the test due to the low stability of GFP (*cf* blue quadrant Fig 5B). Surprisingly the presence of bicarbonate up to 5 mM in the water sample did not affect the sensitivity of Bp BirA-GFP to Cu(II) ions despite significantly increasing the stability and fluorescence of GFP (*cf* red quadrant Fig 5B). This fast and easy-to-use RMIC test for Cu(II) ions only requires a heating block and a UV or blue light source and can be performed as a qualitative or quantitative method in a 96-well plate with a run time of ~10 min.

Metal chelator competition assay

To operate effectively, metal chelators must be selective for a given metal ion over other abundant metal ions and cofactors. Metal-selective chelators are useful tools in biological investigations. EDTA is commonly used as an extracellular zinc chelator [45], for treating lead poisoning and as an anticoagulant. EDTA reversed the effects of Cu(II) and Zn(II) ions on the T_{mP} and T_{mG} values of Bp BirA-GFP. This prompted us to test if Bp BirA-GFP could be used as a screening tool for the identification and characterization of Cu(II) and Zn(II) binding proteins and chelating agents. The screening principle is based on reversal of the Zn(II) and Cu(II) ion effects on Bp BirA-GFP in the presence of a competing metal chelator. We evaluated the sensitivity of this assay with EDTA and BSA [46] due to their strong Zn(II) and Cu(II) binding properties. Here, Bp BirA-GFP (0.5 µM) was reacted with a chelator (10 µM of EDTA or BSA) and either Cu(II) or Zn(II) ions (10 µM). Control DSF-GTP experiments were run in the absence of metal ions or chelators. As expected, EDTA and BSA

clearly reversed the T_{mP} downshift effects of Cu(II) and Zn(II) ions on Bp BirA-GFP demonstrating the utility of this assay format for the detection of chelating agents (Fig 6A-B).

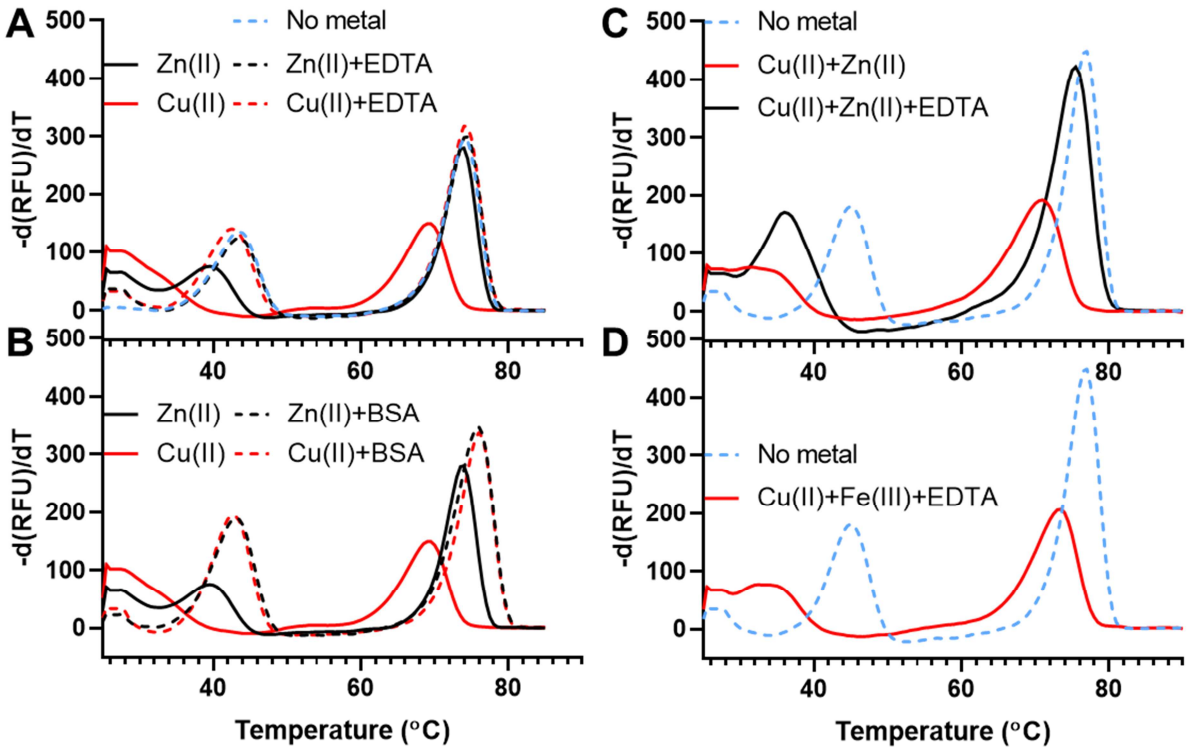

Figure 6: Competitive metal ion binding of EDTA and BSA. Reversal of metal ion effect in the presence of equimolar EDTA (**A**) or BSA (**B**) on Bp BirA-GFP melt curves. A metal chelator competition assay format was set up to determine the metal ion binding preference of EDTA (**C** and **D**) as indicated**.** Combinations of Cu(II), Zn(II) or Fe(II) ions (all at 10 µM) were evaluated in the presence or absence of 10 µM of EDTA or BSA (as indicated) and 0.5 µM Bp BirA-GFP in 25 mM ammonium sulphate (pH 5.7) and 5% glycerol. Control experiments in the absence of metal ions are shown as blue dashed melt curves. Averaged melt curves are presented using GraphPad Prism 8 (N=3).

Next, we examined if we could determine the metal ion binding preference of a chelator such as EDTA which is Fe(III)>>Cu(II)>Zn(II). Here, Bp BirA-GFP (0.5 µM) was reacted with EDTA (10 µM) and combinations of either Cu(II) and Zn(II) or Cu(II) and Fe(III) ions (10 µM each). The affinity of EDTA is ~100 fold higher for Cu(II) than for Zn(II) ions. In this

case, the majority of free ions in solution affecting Bp BirA-GFP will be Zn(II). Our experimental data fit perfectly with the predicted melt curves (*cf* Fig 6A with Fig 6C). EDTA binds with even much higher affinity to Fe(III) ions than Cu(II) ions. Here, the free metal ions in solution affecting Bp BirA-GFP should thus be Cu(II) (*cf* Fig 6A with Fig 6D). Taken together, our data demonstrate the utility of the assay for screening water soluble metal ion chelators and examining their metal ion preference.

5. Conclusions

We identified Bp BirA-GFP as a sensitive Zn(II) and Cu(II) ion sensor when coupled with a DSF signal transduction detection system. The differential metal ion effect on Bp BirA and GFP yielded distinct DSF melt curve signatures allowing identification and quantitation of the metal ion in solution. The dominant metal ion is Cu(II) as it affects both GFP and BirA T_m values to the same extent. Zn(II) and Cu(II) ions have additive effects on Bp BirA T_{mP} but Zn(II) ions do not significantly affect the T_{mG} of GFP at conc ≤ 10 µM. We can further reduce the effect of Zn(II) ions on BirA T_{mP} in the presence of biotin (*cf* Fig 4A). This means that Cu(II) ion concentrations can be determined in the presence of Zn(II) ions ≤ 10 µM (i.e. 20 µM in sample) using the GFP T_{mG} standard curve but the reciprocal is not possible. However, Zn(II) ion concentrations can only be determined when Cu(II) ions are < 1 µM.

Little to no interference was observed in the presence of other tested metal or counter ions. The data obtained with Bp BirA-GFP compared well with ICP-MS in a blind tap water test. In the United States, the Maximum Contaminant Level (MCL) for Cu is 1.3 mg L^{-1} (20.5 µM) in drinking water (National Primary Drinking Water Regulations) and 5 mg L^{-1} (76.5 µM) for Zn (Secondary Drinking Water Standards). Zn(II) and Cu(II) ion concentrations as low as 0.064 mg L^{-1} (i.e. ~1 µM) could be detected with Bp BirA-GFP (Fig 3B). Thus, with its added feature as a simple visual field testing system, we are confident that Bp BirA-GFP

could be developed into a versatile and cost-effective water testing system for Cu(II) ion detection due to its flexible readout formats (i.e. DSF-GTP and isothermal GFP fluorescence quenching methods).

Bp BirA-GFP can be used for screening and identification of metal chelators and further specialized applications are envisaged in serology. For instance, total Zn in serum ranges from 0.66- 1.1 mg L^{-1} (10-17 µM) which is compatible with the detection range of Bp BirA-GFP. Most Zn is protein bound in the serum requiring protein precipitation with trichloracetic acid to release it (e.g. the Wako Zinc kit (Novachem) has a detection range of 4-31 µM). Total Cu in serum ranges from 0.7-1.4 mg L^{-1} (11-22 µM) which is also compatible with the detection range of Bp BirA-GFP. Most test kits require masking agents to distinguish between Cu or Zn. Thus, it is foreseeable that Bp BirA-GFP combined with currently available masking agents could be further developed for testing total Zn and Cu in serum samples allowing further streamlining of medical and veterinary testing in laboratories with real-time PCR capability. The very small sample volumes required would be particularly advantageous in pediatric and small animal serology testing where only limited volumes of liquid biopsies are available.

The sensitivity and dynamic range of the system is set by the concentration of the fluorescent fusion protein and its T_m values. A minor limitation of the system is the relatively long DSF run, but this could be reduced to less than one hour by increasing the ramp speed and shortening the dwell time of the instrument. Reducing the run time could have the benefit of increasing the detection range, with a possible downside being a loss in resolution. The hands-on time is negligible, and the whole process is straightforward and can be automated as liquid and plate-handling systems are routinely available in laboratories. Bp BirA-GFP can be safely used with any real-time PCR instrument used for other sensitive PCR applications with virtually no risk of cross contamination. Although the effect of metal ions can be reversed

with a suitable chelator such as EDTA and BSA, the temperature-dependent detection i.e. DSF-GTP or isothermal fluorescence quenching leads to unfolding and aggregation of Bp BirA-GFP. As such, Bp BirA-GFP can only be used once.

The system is simple yet versatile, and we anticipate that further protein candidates with alternative metal sensitivities will be identified and developed in the future with our DSF-GTP principle to provide a series of new bivalent metal-selective sensors. Although we did not test the system with other fluorescent proteins, we anticipate that GFP could easily be replaced. In this case, combining different fluorescent fusion proteins could pave the way to multiplexing metal ion detection.

References

[1] NHMRC, Australian Drinking Water Guidelines Paper 6 National Water Quality Management Strategy, in: N.R.M.C. National Health and Medical Research Council (Ed.), Commonwealth of Australia, Canberra, 2011.
[2] Copper in Drinking Water, Washington (DC), 2000.
[3] B. Bansod, T. Kumar, R. Thakur, S. Rana, I. Singh, A review on various electrochemical techniques for heavy metal ions detection with different sensing platforms, Biosensors & bioelectronics, 94 (2017) 443-455.
[4] K. Kaur, R. Saini, A. Kumar, V. Luxami, N. Kaur, P. Singh, S. Kumar, Chemodosimeters: An approach for detection and estimation of biologically and medically relevant metal ions, anions and thiols, Coordin Chem Rev, 256 (2012) 1992-2028.
[5] B. Kaur, N. Kaur, S. Kumar, Colorimetric metal ion sensors - A comprehensive review of the years 2011-2016, Coordin Chem Rev, 358 (2018) 13-69.
[6] W.H. Zhou, R. Saran, J.W. Liu, Metal Sensing by DNA, Chem Rev, 117 (2017) 8272-8325.
[7] T.K. Hurst, D. Wang, R.B. Thompson, C.A. Fierke, Carbonic anhydrase II-based metal ion sensing: Advances and new perspectives, Bba-Proteins Proteom, 1804 (2010) 393-403.
[8] C. Isarankura-Na-Ayudhya, T. Tantimongcolwat, H.J. Galla, V. Prachayasittikul, Fluorescent Protein-Based Optical Biosensor for Copper Ion Quantitation, Biological trace element research, 134 (2010) 352-363.
[9] R.B. Thompson, B.P. Maliwal, C.A. Fierke, Fluorescence-based sensing of transition metal ions by a carbonic anhydrase transducer with a tethered fluorophore, Advances in Fluorescence Sensing Technology Iv, Proceedings Of, 3602 (1999) 85-92.
[10] C.Y. Lei, Z. Wang, Z. Nie, H.H. Deng, H.P. Hu, Y. Huang, S.Z. Yao, Resurfaced Fluorescent Protein as a Sensing Platform for Label-Free Detection of Copper(II) Ion and Acetylcholinesterase Activity, Analytical chemistry, 87 (2015) 1974-1980.
[11] A.C. Carpenter, I.T. Paulsen, T.C. Williams, Blueprints for Biosensors: Design, Limitations, and Applications, Genes-Basel, 9 (2018).

[12] T.K. Hurst, D. Wang, R.B. Thompson, C.A. Fierke, Carbonic anhydrase II-based metal ion sensing: advances and new perspectives, Biochimica et Biophysica Acta, 1804 (2010) 393.
[13] J.P. Sumner, N.M. Westerberg, A.K. Stoddard, T.K. Hurst, M. Cramer, R.B. Thompson, C.A. Fierke, R. Kopelman, DsRed as a highly sensitive, selective, and reversible fluorescence-based biosensor for both Cu(+) and Cu(2+) ions, Biosens Bioelectron, 21 (2006) 1302-1308.
[14] Y. Ravikumar, S.P. Nadarajan, C.S. Lee, J.K. Rhee, H.D. Yun, A New-Generation Fluorescent-Based Metal Sensor - iLOV Protein, J Microbiol Biotechnol, 25 (2015) 503-510.
[15] D. Futra, L.Y. Heng, A. Ahmad, S. Surif, T.L. Ling, An optical biosensor from green fluorescent Escherichia coli for the evaluation of single and combined heavy metal toxicities, Sensors (Basel), 15 (2015) 12668-12681.
[16] X.X. Fang, H.L. Li, G.Y. Zhao, X.X. Fang, J.W. Xu, W. Yang, Blue fluorescent protein analogs as chemosensors for Zn2+, Biosensors & bioelectronics, 42 (2013) 308-313.
[17] E.E. Balint, J. Petres, M. Szabo, C.K. Orban, L. Szilagyi, B. Abraham, Fluorescence of a histidine-modified enhanced green fluorescent protein (EGFP) effectively quenched by copper(II) ions, J Fluoresc, 23 (2013) 273-281.
[18] S.P. Nadarajan, Y. Ravikumar, K. Deepankumar, C.S. Lee, H. Yun, Engineering lead-sensing GFP through rational designing, Chem Commun (Camb), 50 (2014) 15979-15982.
[19] X. Yu, M.P. Strub, T.J. Barnard, N. Noinaj, G. Piszczek, S.K. Buchanan, J.W. Taraska, An engineered palette of metal ion quenchable fluorescent proteins, PloS one, 9 (2014) e95808.
[20] L. Shi, Y. Li, Z. Liu, T.D. James, Y. Long, Simultaneous determination of Hg(II) and Zn(II) using a GFP inspired chromophore, Talanta, 100 (2012) 401-404.
[21] P.N. Basa, A.G. Sykes, Differential sensing of Zn(II) and Cu(II) via two independent mechanisms, The Journal of organic chemistry, 77 (2012) 8428-8434.
[22] L. Qu, C. Yin, F. Huo, J. Chao, Y. Zhang, F. Cheng, A pyridoxal-based dual chemosensor for visual detection of copper ion and fluorescent detection of zinc ion, Sensors and Actuators B: Chemical, 191 (2014) 158-164.
[23] K. Kluska, J. Adamczyk, A. Krezel, Metal binding properties of zinc fingers with a naturally altered metal binding site, Metallomics, 10 (2018) 248-263.
[24] K. Kluska, J. Adamczyk, A. Krezel, Metal binding properties, stability and reactivity of zinc fingers, Coordin Chem Rev, 367 (2018) 18-64.
[25] G.K. Walkup, B. Imperiali, Fluorescent chemosensors for divalent zinc based on zinc finger domains. Enhanced oxidative stability, metal binding affinity, and structural and functional characterization, Journal of the American Chemical Society, 119 (1997) 3443-3450.
[26] M.J.J. Moreau, I. Morin, S.P. Askin, A. Cooper, N.J. Moreland, S.G. Vasudevan, P.M. Schaeffer, Rapid determination of protein stability and ligand binding by differential scanning fluorimetry of GFP-tagged proteins, Rsc Adv, 2 (2012) 11892-11900.
[27] M.J. Moreau, P.M. Schaeffer, Dissecting the salt dependence of the Tus–Ter protein–DNA complexes by high-throughput differential scanning fluorimetry of a GFP-tagged Tus, Mol Biosyst, 9 (2013) 3146-3154.
[28] A.E. Sorenson, P.M. Schaeffer, High-Throughput Differential Scanning Fluorimetry of GFP-Tagged Proteins, Methods Mol Biol, 2089 (2020) 69-85.
[29] S. Askin, T.E.H. Bond, A.E. Sorenson, M.J.J. Moreau, H. Antony, R.A. Davis, P.M. Schaeffer, Selective protein unfolding: a universal mechanism of action for the development of irreversible inhibitors, Chem Commun (Camb), 54 (2018) 1738-1741.
[30] T.E.H. Bond, A.E. Sorenson, P.M. Schaeffer, Functional characterisation of Burkholderia pseudomallei biotin protein ligase: A toolkit for anti-melioidosis drug development, Microbiological research, 199 (2017) 40-48.
[31] S.P. Askin, T.E.H. Bond, P.M. Schaeffer, Green fluorescent protein-based assays for high-throughput functional characterization and ligand-binding studies of biotin protein ligase, Anal Methods-Uk, 8 (2016) 418-424.

[32] T.E.H. Bond, A.E. Sorenson, P.M. Schaeffer, A green fluorescent protein-based assay for high-throughput ligand-binding studies of a mycobacterial biotin protein ligase, Microbiological research, 205 (2017) 35-39.
[33] M.J. Moreau, I. Morin, P.M. Schaeffer, Quantitative determination of protein stability and ligand binding using a green fluorescent protein reporter system, Mol Biosyst, 6 (2010) 1285-1292.
[34] M.J. Moreau, P.M. Schaeffer, Differential Tus-Ter binding and lock formation: implications for DNA replication termination in Escherichia coli, Mol Biosyst, 8 (2012) 2783-2791.
[35] R.L. Zheng, T.M. Jenkins, R. Craigie, Zinc folds the N-terminal domain of HIV-1 integrase, promotes multimerization, and enhances catalytic activity, Proceedings of the National Academy of Sciences of the United States of America, 93 (1996) 13659-13664.
[36] T.L. Yap, T. Xu, Y.L. Chen, H. Malet, M.P. Egloff, B. Canard, S.G. Vasudevan, J. Lescar, Crystal structure of the dengue virus RNA-dependent RNA polymerase catalytic domain at 1.85-Angstrom resolution, Journal of virology, 81 (2007) 4753-4765.
[37] S.L.J. Michel, J.M. Berg, Building a metal binding domain, one half at a time, Chem Biol, 9 (2002) 667-668.
[38] T. Nittis, G.N. George, D.R. Winge, Yeast Sco1, a protein essential for cytochrome c oxidase function is a Cu(I)-binding protein, The Journal of biological chemistry, 276 (2001) 42520-42526.
[39] J.K. Nyborg, O.B. Peersen, That zincing feeling: the effects of EDTA on the behaviour of zinc-binding transcriptional regulators, The Biochemical journal, 381 (2004) e3-4.
[40] I. Paul, J. Cui, E.L. Maynard, Zinc binding to the HCCH motif of HIV-1 virion infectivity factor induces a conformational change that mediates protein-protein interactions, Proceedings of the National Academy of Sciences of the United States of America, 103 (2006) 18475-18480.
[41] P. Cimmperman, L. Baranauskiene, S. Jachimoviciute, J. Jachno, J. Torresan, V. Michailoviene, J. Matuliene, J. Sereikaite, V. Bumelis, D. Matulis, A quantitative model of thermal stabilization and destabilization of proteins by ligands, Biophysical journal, 95 (2008) 3222-3231.
[42] A. Kaufman Katz, L. Shimoni-Livny, O. Navon, N. Navon, C.W. Bock, J.P. Glusker, Copper-binding motifs: structural and theoretical aspects, Helv Chim Acta, 86 (2003) 1320-1338.
[43] D. Wyrzykowski, L. Chmurzynski, Thermodynamics of citrate complexation with Mn2+, Co2+, Ni2+ and Zn2+ ions, J Therm Anal Calorim, 102 (2010) 61-64.
[44] R.B. Martin, Ph as a Variable in Free Zinc Ion Concentration from Zinc-Containing Lozenges, Antimicrobial Agents and Chemotherapy, 32 (1988) 608-609.
[45] R.J. Radford, S.J. Lippard, Chelators for investigating zinc metalloneurochemistry, Current Opinion in Chemical Biology, 17 (2013) 129-136.
[46] J. Masuoka, P. Saltman, Zinc(Ii) and Copper(Ii) Binding to Serum-Albumin - a Comparative-Study of Dog, Bovine, and Human Albumin, Journal of Biological Chemistry, 269 (1994) 25557-25561.

Highlights

- *Burkholderia pseudomallei* biotin protein ligase senses copper and zinc ions in water
- GFP-tagged biotin protein ligase differentiates between copper and zinc ions
- The assay format allows high-throughput screening of metal chelating agents
- A simple visual in-field water testing format was devised for copper ion detection
- Recommended maximum impurity concentrations of copper are easily detected in water

Conflict of interest

None.

Author statement

Alanna Sorenson: Conceptualization, Methodology, Investigation, Visualization, Formal analysis, Writing - Reviewing and Editing **Patrick Schaeffer:** Conceptualization, Project administration, Methodology, Visualization, Formal analysis, Writing - Reviewing and Editing, Funding acquisition

Declaration of interests

☒ The authors declare that they have no known competing financial interests or personal relationships that could have appeared to influence the work reported in this paper.

☐The authors declare the following financial interests/personal relationships which may be considered as potential competing interests: